Proceedings of FEDSM2009
ASME 2009 Fluids Engineering Division Summer Meeting
August 2-5, 2009, Vail, Colorado USA

FEDSM2009-78166

PARALLEL FLOW IN ORDERED FIBROUS STRUCTURES: AN ANALYTICAL APPROACH

A. Tamayol
PhD Student
Ata42@sfu.ca

M. Bahrami
Assistant Professor
mbahrami@sfu.ca

Mechatronic Systems Engineering,
School of Engineering Science,
Simon Fraser University, BC, Canada

ABSTRACT

In this study, fully-developed flow parallel to ordered fibrous structures is investigated analytically. The considered fibrous media are made up of in-line (square), staggered, and hexagonal arrays of cylinders. Starting from the general solution of Poisson's equation, compact analytical solutions are proposed for both velocity distribution and permeability of the considered structures. In addition, independent numerical simulations are performed for the considered patterns over the entire range of porosity and the results are compared with the proposed solutions. The developed models are successfully verified through comparison with existing experimental data, collected by others, and the present numerical results over a wide range of porosity. The results show that for the ordered arrangements with high porosity, the parallel permeability is independent of the microstructure geometry; on the other hand, for lower porosities the hexagonal arrays results in lower pressure drop, as expected.

NOMENCLATURE

d = Fiber diameter, m

K = Viscous permeability, m^2

K^* = Dimensionless viscous permeability, $K^* = K / d^2$

P = Pressure, Pa

Q = Volumetric flow rate, m^3 / s

r_0 = Fiber radius, m

S = Distance between adjacent fibers, m

U_D = Volume-averaged superficial velocity, m/s

w = Velocity in z -direction, m/s

Greek symbols

ε = Porosity

μ = Fluid viscosity, $N\,s/m^2$

φ = Solid volume fraction, $\varphi = 1 - \varepsilon$

ε = Porosity

1 INTRODUCTION

Transport phenomena in porous media have been the focus of numerous studies since the 1850s, which indicates the importance of this topic. Most of these studies refer to granular materials with low and medium porosities, $0.3 < \varepsilon < 0.6$. Comprehensive reviews of the pertinent literature are presented by Kaviany [1], Nield and Bejan [2], and Dullien [3]. Fibrous structures, made up of cylindrical-like particles, can form stable geometries with high porosity, up to 0.99 [4]. Moreover, these fibrous structures feature low-weight, high surface-to-volume ratios, and high heat transfer coefficients [4]. Fibrous porous materials have applications in several engineering areas including: filtration and separation of particles [5], composite fabrication [6], heat exchangers [4,7], and fuel cells [8]. Experimental observations have shown that a linear relationship exists between the volume-averaged superficial fluid velocity and the pressure gradient; this is called Darcy's law [1]:

$$-\nabla P = \frac{\mu}{K} U_D \qquad (1)$$

where μ is the fluid viscosity and K is the viscous permeability of the medium. Viscous permeability can be interpreted as the ability of the porous matrix to pass fluids. Macroscopic transport properties such as permeability and heat transfer coefficient are functions of geometrical features of the porous medium; thus, determination of exact transport

properties for real fibrous materials with random structures is very complex and in many cases not possible. However, several researchers have argued that the parallel permeability of unidirectional fibers can provide an upper bound for the permeability of real structures [9]. Moreover, a blend of normal and parallel permeabilities of unidirectional arrangements provides an estimate for the permeability of random fibrous media, e.g., Jackson and James [10] and Happel and Brenner [11]. Therefore, a detailed analysis of parallel permeability of unidirectional fibers is valuable.

Happel [12] and Sparrow and Loeffler [13] studied parallel permeability for unidirectional cylinders for heat exchanger application. Happel [12] assumed a circular unit cell with a single cylinder located at its center and applied zero-shear stress boundary condition on the outer surface of the control volume; this method is called the limited boundary layer approach. However, the model of [12] cannot accurately predict the parallel permeability for lower porosities where neighboring fibers play an important role [10].

Sparrow and Loeffler [13], on the other hand, considered both square and staggered arrangements of monodispersed fibers. They used the general solution of Poisson's equation in the cylindrical coordinate system and applied the boundary conditions at finite discrete points. The evaluated coefficients in their series solution were functions of porosity; therefore, they proposed an approximate compact relationship which was claimed to be accurate only for highly porous structures, $\varepsilon >$ 0.9 [13]. The approximate model of [13], for staggered arrangement, was identical to the model of Happel [12]. Velocity distribution was also reported in a tabular form, which is not easy-to-use. Later, Drummond and Tahir [14] performed a comprehensive analytical investigation of normal and parallel flows for various ordered arrays of fibers. For parallel flow, they started from the general solution of Poisson's equation in the form of a series. Drummond and Tahir [14] claimed that their singularity method was more accurate than the approach of Sparrow and Loeffler [13].

However, their models [14] for normal flow were not accurate [15]. Drummond and Tahir [14] did not report explicit relationships for the velocity distribution. Observing the similarity between the final relationship for the parallel permeability proposed by Happel [12] and those derived in their analyses for different fiber arrangements, Drummond and Tahir [14] concluded that any correlation proposed for the parallel permeability should have the following form:

$$K^* = \frac{K}{d^2} = \left(2\varphi - \frac{\varphi^2}{2} - \ln\varphi - C \right) \frac{1}{16\varphi} \qquad (2)$$

where φ is the solid volume fraction, d is the fibers diameter, and C is a constant that should be determined empirically. For C=1.5, Eq. (2) yields the model of Happel [12] and Sparrow and Loeffler [13]. Recently, Tamayol and Bahrami [16] assumed a parabolic velocity distribution and using an integral technique determined the normal and parallel permeabilities of square arrays of cylinders. Their model for normal flow was able to capture the trend of experimental data from several sources. The proposed relationship for parallel permeability was in good agreement with the model of Happel [12] in the upper limit of porosity and for the lower limit it was in agreement with experimental data. In a subsequent work, Tamayol and Bahrami [17] performed a comprehensive numerical study and reported the normal and the parallel permeability of square fiber arrangements over a wide range of porosity. Comparison of the numerical results with their analytical relationship showed that although their model could capture the trends of numerical results, the differences were significant in the medium range of porosity $0.5 < \varepsilon < 0.8$ [17]. Comparing the numerical velocity distribution with the parabolic profile, Tamayol and Bahrami [17] argued that the assumption of parabolic velocity distribution was not accurate. Therefore, the objectives of the present study are:

1) To develop accurate velocity profiles for square and staggered arrays of fibers.

2) To find compact and accurate models for parallel permeability in unidirectional fibrous matrices.

In this study, porous material is assumed to be periodic and is represented by a 3-dimensional unit cell. Following [13], governing equations are solved analytically and velocity distributions are reported for square, staggered, and hexagonal arrays of fibers. Moreover, employing an integral technique, compact models are developed for parallel permeability. Due to a lack of experimental and numerical data for parallel flow in unidirectional arrangements, numerical simulations are also performed using Fluent software [18], over the entire range of porosity to validate the models.

2 GEOMETRICAL MODELING

Following the approach used successfully in several applications such as spherical packed beds [19], gas diffusion layer of fuel cells [20], and fibrous media [21-27] a representative unit cell is considered to analyze the geometry of the fibrous media. The unit cell (or basic cell) is the smallest volume which can represent characteristics of the whole microstructure. In the following sub-sections, various ordered arrangements, shown in Fig. 1, will be investigated.

According to symmetry lines, only the selected portions of the unit cells are considered in the analysis. Based on geometry, the solid volume fraction and porosity of square and staggered arrays are:

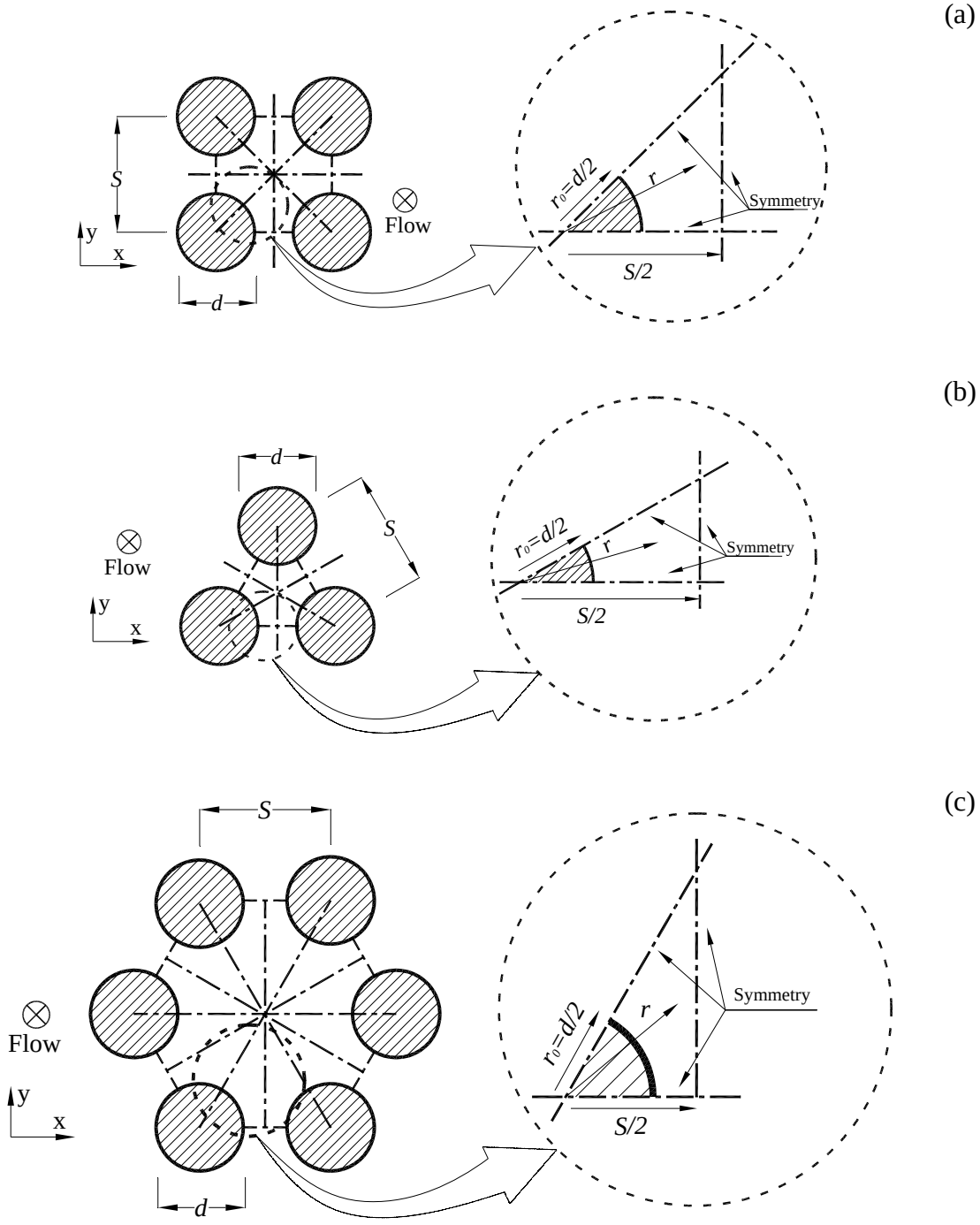

Figure 1: Unit cell for a) square, b) staggered, and c) hexagonal arrangements.

$$\varphi = 1 - \varepsilon = \frac{\pi d^2}{4S^2} \quad \text{Square}$$
$$\varphi = 1 - \varepsilon = \frac{\pi d^2}{2\sqrt{3}S^2} \quad \text{Staggered} \qquad (3)$$
$$\varphi = 1 - \varepsilon = \frac{\pi d^2}{3\sqrt{3}S^2} \quad \text{Hexagonal}$$

Therefore, the minimum possible values of ε for square, staggered, and hexagonal arrangements with no overlapping are 0.215, 0.094, and 0.395, respectively.

3 VELOCITY DISTRIBUTION

Laminar, steady, and fully-developed flow parallel to square, staggered, hexagonal fiber arrangements, shown in Fig. 1, is investigated. Darcy's relationship, Eq. (1), holds when the flow

passing through pores is in creeping regime, i.e., inertial effects are negligible [1]. However, the present models are valid for laminar fully-developed flows with higher Reynolds numbers. Applying the abovementioned assumptions, the conservation of linear momentum leads to Poisson's equation:

$$\frac{\partial^2 w}{\partial r^2}+\frac{\partial w}{r\partial r}+\frac{\partial^2 w}{r^2\partial\theta^2}=\frac{1}{\mu}\left(\frac{dP}{dz}\right) \tag{4}$$

where w is the component of velocity in the z-direction. The general solution of this equation is [28]:

$$w = A + B\ln r + \frac{r^2}{4\mu}\left(\frac{dP}{dz}\right) + \\ + \sum_{k=1}^{\infty}\left(C_k r^k + D_k r^{-k}\right)\left(E_k\cos k\theta + F_k \sin k\theta\right) \tag{5}$$

For square arrangement, symmetry lines are located at $\theta = 0$ and $\theta = \pi/4$. The first condition results in $F_k = 0$ and the second condition holds when k = 4, 8, 12, … . The no-slip boundary condition on the solid walls leads to:

$$D_k = C_k {r_0}^{2k} \text{ and } A = -B\ln r_0 - \frac{{r_0}^2}{4\mu}\left(\frac{dP}{dz}\right) \tag{6}$$

Total frictional force exerted on the fluid by solid rods must be balanced by the net pressure force acting over the entire cross-section of the basic cell:

$$\int_0^{\pi/4}\mu\left(\frac{\partial w}{\partial r}\right)_{r=r_0} r_0\, d\theta = \int_0^{\pi/4}\int_{r_0}^{S/2\cos\theta}\left(\frac{dP}{dz}\right) r\, dr\, d\theta \tag{7}$$

Using this integral, the constant B can be found:

$$B = -\frac{S^2}{2\pi\mu}\left(\frac{dP}{dz}\right) \tag{8}$$

Consequently, the velocity distribution becomes:

$$w^* = \left[\frac{2S^2}{\pi d^2}\ln\eta - \frac{\eta^2-1}{4} + \right. \\ \left. \sum_{k=1}^{\infty}\frac{G_k\, d^{4k-2}}{2^{4k}}\left(\eta^{4k}-\eta^{-4k}\right)\cos 4k\theta\right] \\ w^* = \frac{w}{-\frac{d^2}{4\mu}\left(\frac{dP}{dz}\right)} \quad , \quad \eta = \frac{r}{d/2} \tag{9}$$

The last constant, G_k, is found by applying the symmetry condition on the border where $r = S/(2\cos\theta)$. Therefore, one can write:

$$\frac{2}{\pi}(\cos\theta)^2 - \frac{1}{2} + \\ \sum_{k=1}^{\infty}\frac{g_k}{\cos\theta^{4k-1}}\left[\cos(4k-1)\theta + \left(\frac{d\cos\theta}{S}\right)^{8k}\cos(4k+1)\theta\right] = 0 \tag{10}$$

where:

$$g_k = G_k\, 4k\left(\frac{S}{2}\right)^{4k-2} \tag{11}$$

Sparrow and Loeffler [13] applied Eq. (10) at a finite number of points along the boundary and solved the resulting set of linear equations to determine the unknown coefficients, i.e., g_k. The same approach is followed here and the calculated coefficients for several porosities are listed in Table 1. The listed values are in agreement with the values reported by Sparrow and Loeffler [13].

The triangular unit cell section for the staggered fiber arrangements is shown in Fig 1b. The symmetry boundaries are located at $\theta = 0$ and $\theta = \pi/6$. The governing equation and its general solution are still Eqs. (4) and (5). Following the same procedure used in the previous sub-section and applying symmetry boundary conditions leads to:

$$w^* = \left[\frac{\sqrt{3}S^2}{\pi d^2}\ln\eta - \frac{\eta^2-1}{4} + \right. \\ \left. \sum_{k=1}^{\infty}\frac{g_k}{6k}\left(\frac{d}{S}\right)^{6k-2}\left(\eta^{6k}-\eta^{-6k}\right)\cos 6k\theta\right] \tag{12}$$

The unknown coefficients are evaluated with the same approach used for square arrangements and the results as listed in Table 1.

Following the same approach and considering the location of the symmetry lines for hexagonal arrays at $\theta = 0$ and $\theta = \pi/3$, the velocity distribution can be found as:

$$w^* = \left[\frac{3\sqrt{3}S^2}{2\pi d^2}\ln\eta - \frac{\eta^2-1}{4} + \right. \\ \left. \sum_{k=1}^{\infty}\frac{g_k}{3k}\left(\frac{d}{S}\right)^{3k-2}\left(\eta^{3k}-\eta^{-3k}\right)\cos 3k\theta\right] \tag{13}$$

The unknown coefficients are listed in Table 1. From the listed coefficients in Table 1 and the form of the series solutions in Eqs. (9), (12) and (13), it is expected that truncating the series from the second term, does not affect the velocity distributions significantly. Our analysis also showed that substituting g_1 with an average value has a negligible impact on the predicted results (less than 4 percent). Therefore, g_1 is replaced by -0.107, -0.0437, and -0.246 for square, staggered, and hexagonal arrangements, respectively. Hence, the velocity distribution will be:

Table 1: Calculated coefficients in velocity distribution.

Square arrangement						
S/d	ε	g_1	g_2	g_3	g_4	g_5
4.0	0.95	-0.1253	-0.0106	-0.0006	0	0
2.0	0.80	-0.1250	-0.0105	-0.0006	0	0
1.5	0.65	-0.1225	-0.0091	-0.0002	0	0
1.2	0.45	-0.1104	-0.0024	-0.0015	0.0003	0
1.1	0.35	-0.0987	0.0036	0.0029	0.0005	0
1.05	0.29	-0.0904	0.0073	0.0032	0.0002	0
Staggered arrangement						
S/d	ε	g_1	g_2	g_3	g_4	g_5
4.0	0.94	-0.0505	-0.0008	0.0000	0	0
2.0	0.77	-0. 0505	-0.0008	0.0000	0	0
1.5	0.60	-0. 0502	-0.0007	0.0001	0	0
1.2	0.37	-0. 0469	0.0007	0.0002	0.0000	0
1.1	0.25	-0.0416	0.0028	0.0004	0.0000	0
1.05	0.18	-0.0368	0.0043	0.0003	-0.0001	0.0000
Hexagonal arrangement						
S/d	ε	g_1	g_2	g_3	g_4	g_5
4.0	0.96	-0.2850	-0.0365	-0.0048	-0.0006	-0.0001
2.0	0.85	-0.2827	-0.0350	-0.0043	-0.0005	0.0000
1.5	0.73	-0.2728	-0.0286	-0.0019	0.0002	0.0001
1.2	0.58	-0.2433	-0.0096	0.0053	0.0021	0.0006
1.1	0.50	-0.2216	0.0038	0.0093	0.0029	0.0004
1.05	0.45	-0.2076	0.0116	0.0103	0.0027	-0.0003

$$w^* = \begin{cases} \left[\dfrac{2S^2}{\pi d^2}\ln\eta - \dfrac{\eta^2-1}{4} - \dfrac{0.0287\,d^2}{S^2}\left(\eta^4-\eta^{-4}\right)\cos 4\theta\right] & \text{Square} \\ \left[\dfrac{\sqrt{3}\,S^2}{\pi d^2}\ln\eta - \dfrac{\eta^2-1}{4} - \dfrac{0.007\,d^4}{S^4}\left(\eta^6-\eta^{-6}\right)\cos 6\theta\right] & \text{Staggered} \\ \left[\dfrac{3\sqrt{3}\,S^2}{2\pi d^2}\ln\eta - \dfrac{\eta^2-1}{4} - \dfrac{0.082\,d}{S}\left(\eta^3-\eta^{-3}\right)\cos 3\theta\right] & \text{Hexagonal} \end{cases} \quad (14)$$

3.1 NUMERICAL SIMULATION

Due to the lack of experimental and numerical data for parallel flow through ordered arrangements of fibers [15], a numerical study is performed using Fluent software [18] to verify the solution. To find fully-developed velocity profiles, the length of the cylinders is large enough to result in a fully developed velocity profile. Structured grids are generated using Gambit [18], the preprocessor in the Fluent [18] package; numerical grid aspect ratios are kept in the range of 1-5. Fluent [18] is a finite volume based code and second order upwind scheme is selected to discretize the governing equations. SIMPLE algorithm is employed for pressure-velocity coupling. The inlet

velocity of the media is assumed to be uniform. Constant pressure boundary condition is applied on the computational domain outlet. The symmetry boundary condition is applied on the side borders of the unit cells. Grid independence is tested for different cases and the size of computational grids used for each geometry is selected such that the maximum difference in the predicted values for pressure gradient is less than 2%. The convergence criterion, maximum relative error in the value of dependent variables between two successive iterations, is set at 10^{-6}.

To verify the proposed velocity distribution for the square arrangements, numerical and analytical velocity profiles are plotted in Figs. 2-4 for square and staggered arrangements with different porosities. The velocity magnitudes are nondimensionalized using the volume averaged velocity, U_D. These figures indicate that Eq. (14) accurately predicts the velocity distribution in the considered geometries.

4) PERMEABILITY

Velocity distributions are developed analytically for parallel flow through square, staggered, and hexagonal arrays of cylinders in previous sections. Moreover, the flow-fields are solved numerically to verify the theoretical results. The volumetric flow rate that passes the medium is found by integrating Eq. (14) over the pore area. Substituting for dP/dz from Darcy's equation and using the solid volume fraction definitions for square arrangement of fibers, the non-dimensional permeability is simplified as:

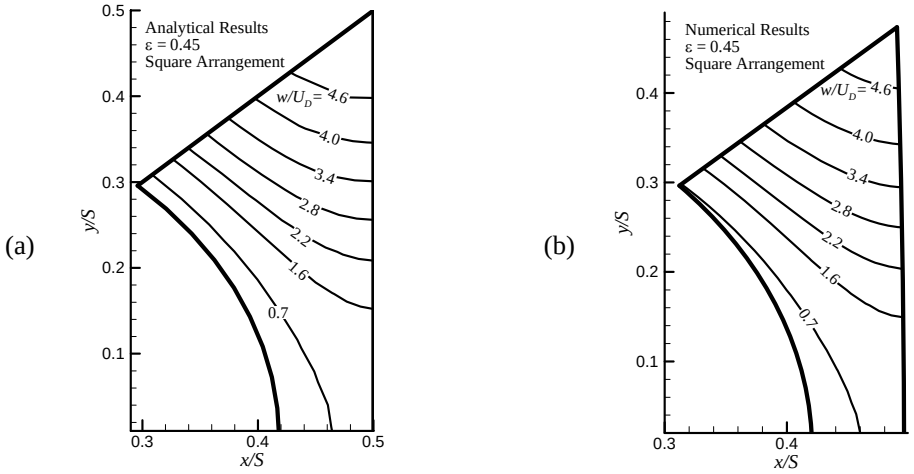

Figure 2: Present velocity distributions for a square arrangement with $\varepsilon = 0.45$, a) analytical (Eq. (14)) and b) numerical.

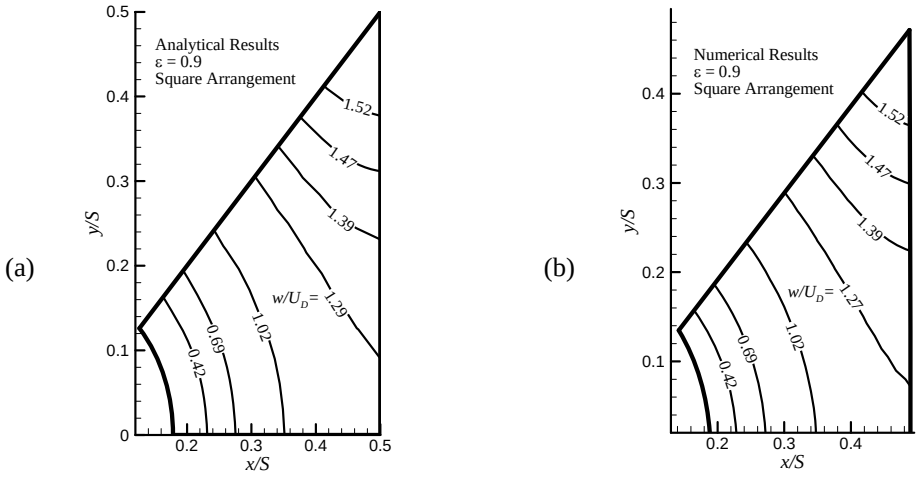

Figure 3: Present velocity distributions for a square arrangement with $\varepsilon = 0.9$, a) analytical (Eq. (14)) and b) numerical.

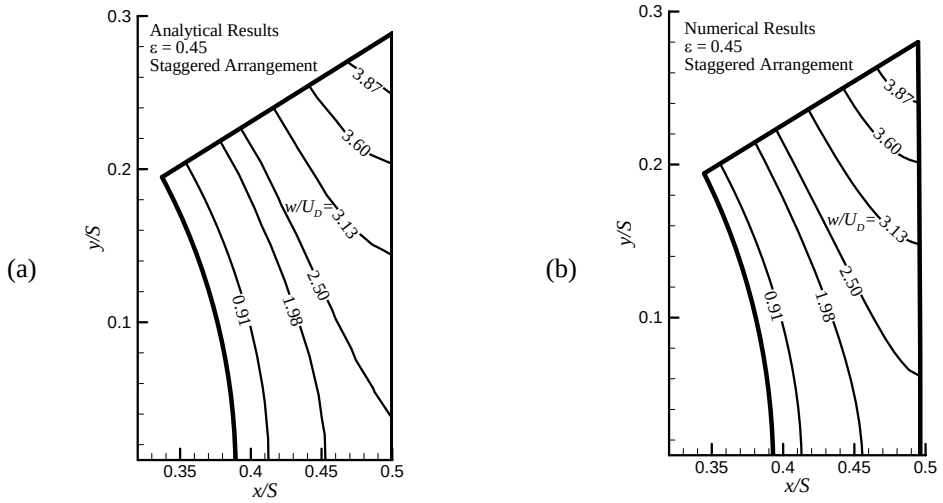

Figure 4: Present velocity distributions for staggered arrangement of cylinders with $\varepsilon = 0.45$ a) analytical (Eq. (14)) and b) numerical.

$$K^* = \frac{K}{d^2} = \begin{cases} \frac{1}{16\varphi}\left[-1.479 - \ln\varphi + 2\varphi - \frac{\varphi^2}{2} - 0.0186\varphi^4\right] & \text{Square} \\ \frac{1}{16\varphi}\left[-1.498 - \ln\varphi + 2\varphi - \frac{\varphi^2}{2} - 0.0018\varphi^6\right] & \text{Staggered} \\ \frac{1}{16\varphi}\left[-1.354 - \ln\varphi + 2\varphi - \frac{\varphi^2}{2} - 0.026\varphi^3\right] & \text{Hexagonal} \end{cases} \quad (15)$$

To verify the proposed model for parallel permeability of square arrays, Eq. (15), and numerical results are plotted in Fig. 5. In addition, experimental data of Sullivan [29] and Skartsis et al. [30] and the numerical results reported by Sangani and Yao [16] are included. Figure 5 shows that the present model is in agreement with the experimental and the numerical data. The accuracy of the developed model is also compared with the model of Drummond and Tahir's results [14] in Table 2. It can be seen that the maximum difference of the present model with numerical and experimental data is less than 8%. The present solution is compared with the analytical models of Happel [12] and Tamayol and Bahrami [16] in Fig. 6. As shown in Fig. 6 and Table 2 the present model accurately predicts the numerical results. More importantly, the present solution enables one to predict the velocity distribution in the unit cell. Although the model of Drummond and Tahir [14] is accurate, they did not provide a compact relationship for the velocity distribution.

In Fig. 7 the present model is compared with the numerical results and one experimental data point reported by Sullivan [29]. It can be seen that the model captures the numerical and the experimental results over the entire range of porosity. The present model is also depicted against analytical models of Happel [12] and Drummond and Tahir [14] in Fig. 8. This figure shows that the present model is the only one that is accurate over the entire range of porosity; especially, in lower porosities were the other models fail. To avoid misjudgments due to log-scale plots, the predicted values of Eq. (15) and the model of Drummond and Tahir [14] over the entire range of porosity are also listed in Table 3. It can be seen that only the present solution predicts numerical results within 10% accuracy and the model of [14] is not accurate in low porosities.

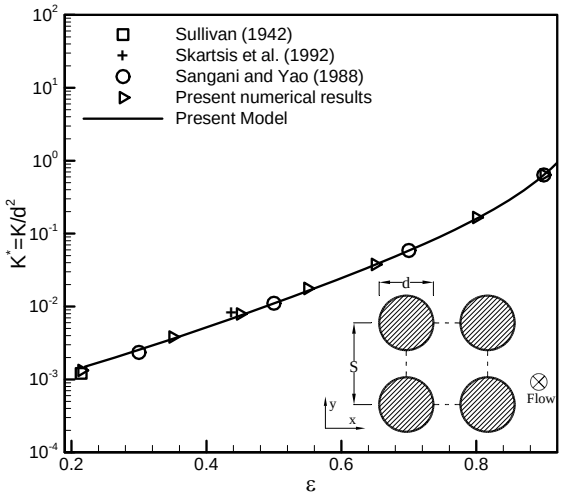

Figure 5: Comparison of the proposed model with the numerical and experimental results, square arrangement.

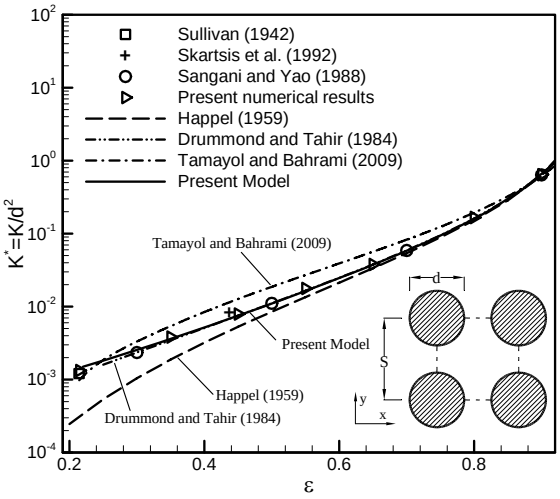

Figure 6: Comparison of the proposed model with other existing models, square arrangement.

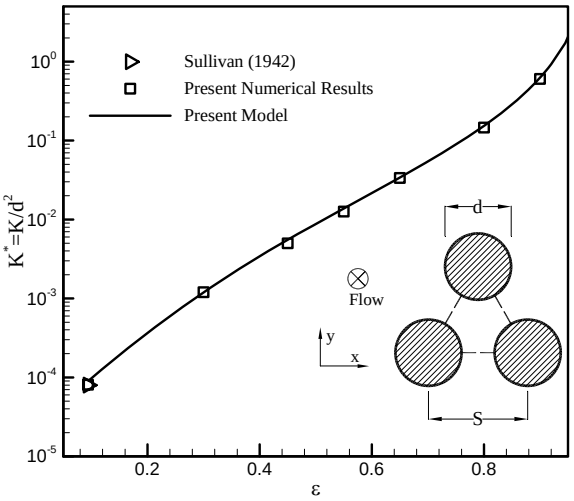

Figure 7: Comparison of the proposed model with the numerical and experimental results, staggered arrangement.

Table 2: Comparison between accuracy of different models for square arrangement.

ε	K/d^2 Numerical	K/d^2 Tamayol and Bahrami [16]	Difference (%)	K/d^2 Drummond and Tahir [14]	Difference (%)	K/d^2 Present model	Difference (%)
0.215	0.0013	0.0010	34.8	0.0012	8.8	0.0014	8.2
0.35	0.0038	0.0054	29.1	0.0035	10.4	0.0036	6.2
0.45	0.0079	0.0127	37.7	0.0075	5.4	0.0075	5.4
0.55	0.0177	0.0271	34.5	0.0165	7.3	0.0164	8.4
0.65	0.0378	0.0565	33.1	0.0378	0.1	0.0374	1.0
0.8	0.1667	0.1938	14.0	0.1603	4.0	0.1596	4.4
0.9	0.6429	0.6170	4.2	0.6383	0.7	0.6368	1.0

$$\text{Difference} = \frac{\left|\text{Model} - \text{Present numerical}\right|}{\text{Model}} \times 100$$

Table 3: Comparison between accuracy of different models for staggered arrangement.

ε	K/d^2 Numerical	K/d^2 Present model	Difference (%)	K/d^2 Drummond and Tahir [14]	Difference (%)
0.094	0.000081	0.000090	10.0	0.000132	38.5
0.3	0.0012	0.001204	2.2	0.001284	4.2
0.45	0.0050	0.005516	9.0	0.005627	10.8
0.55	0.0126	0.013784	8.9	0.013922	9.8
0.65	0.0336	0.034030	1.3	0.034208	1.8
0.8	0.1463	0.153570	4.7	0.15389	4.9
0.9	0.6039	0.624740	3.3	0.62537	3.4

$$\text{Difference} = \frac{\left|\text{Model} - \text{Present numerical}\right|}{\text{Model}} \times 100$$

The present analytical solution, present numerical results, the models of Drummond and Tahir [14] and Happel [12] for hexagonal arrangement are compared in Fig. 9. As listed in Table 4, the proposed relationship for permeability of hexagonal arrays captures numerical results within 9% accuracy.

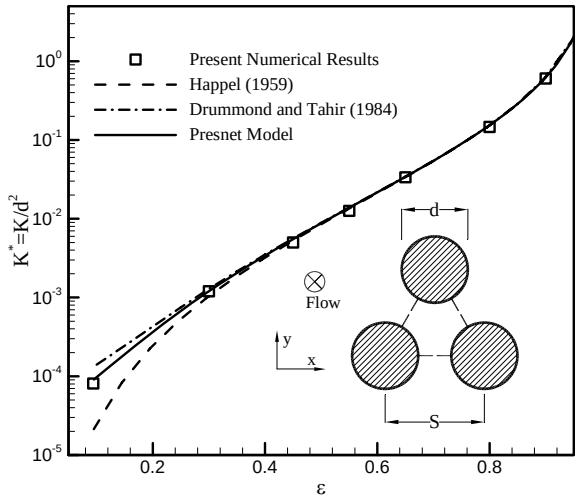

Figure 8: Comparison of the proposed model with other existing models, staggered arrangement.

5 EFFECTS OF FIBER ARRANGEMENT ON PERMEABILITY

Comparing the relationships for dimensionless permeability of various arrangements, given in Eq. (15), one can see that the differences are in the constants and the higher order terms. The higher order terms become negligible for highly porous structures, i.e., $\varphi \to 0$. Therefore, it is expectable that the three equations lead to almost identical values in this limit. Note that for lower porosities, the effect of higher order terms is considerable and staggered arrays have the lowest permeability, see Fig 10. For $\varepsilon > 0.85$ the difference between the two models is less than 5%.

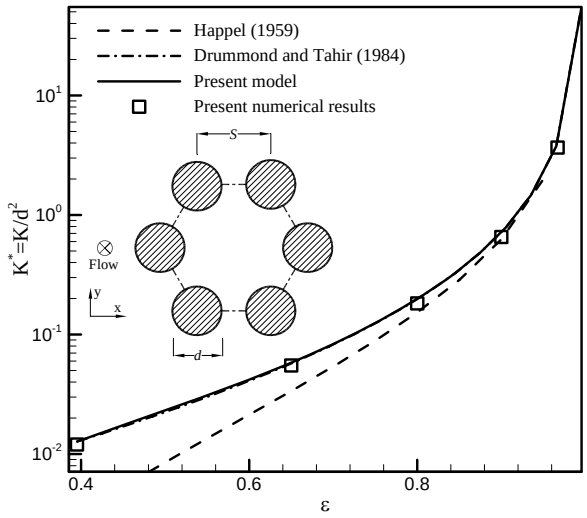

Figure 8: Comparison of the proposed model with other existing models, hexagonal arrangement.

6 SUMMARY AND CONCLUSIONS

Fluid flow parallel to staggered, square, hexagonal arrays of cylinders is studied both analytically and numerically. A truncated form of the series solution of Poisson's equation provides accurate results for velocity distribution in the investigated channel-like geometries. Using the proposed solutions, compact models are developed for permeability of the media.

Independent numerical simulations are performed to verify the solutions for velocity distribution and permeability. The present approach captures the numerical results for permeability within maximum 10% accuracy for the considered arrangements, respectively. Fiber arrangement has negligible effect on the pressure drop and permeability for high porosities, $\varepsilon > 0.85$. On the other hand, for lower porosities the effect of microstructure is significant and staggered arrays have lower permeability than other arrangements. As such, use of hexagonal arrays of tube in heat exchangers reduces the consequent pressure drop.

Table 4: Comparison between accuracy of different models for hexagonal arrangement.

ε	K/d^2 Numerical	K/d^2 Present model	Difference (%)	K/d^2 Drummond and Tahir [14]	Difference (%)
0.395	0.012	0.013	8.6	0.013	8.7
0.65	0.055	0.058	6.3	0.057	4.8
0.80	0.182	0.199	8.4	0.198	8.1
0.90	0.654	0.716	8.6	0.715	8.5
0.967	3.663	4.024	9.0	4.021	8.9

$$\text{Difference} = \frac{\left|\text{Model} - \text{Present numerical}\right|}{\text{Model}} \times 100$$

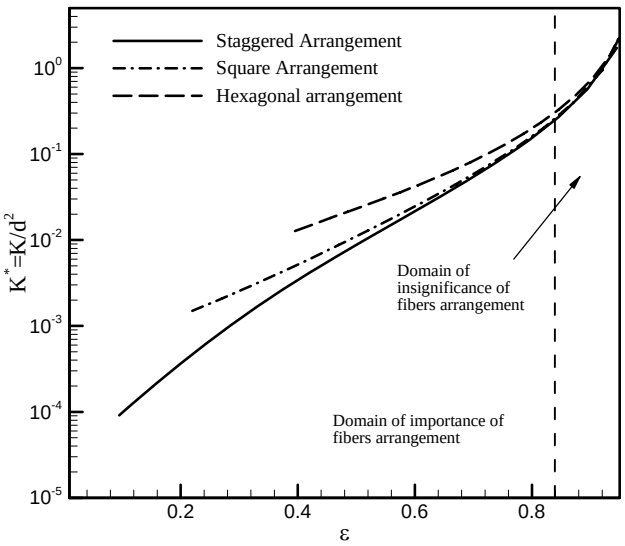

Figure 10: Effect of arrangement on the permeability.

7 ACKNOWLEDGMENTS

The authors gratefully acknowledge the financial support of the Natural Sciences and Engineering Research Council of Canada (NSERC).

8 REFERENCES

[1] Kaviany, M., 1992, "Principles of Heat Transfer in Porous Media," Springer-Verlag, New York.

[2] Nield, D.A. and Bejan, A., 1992, "Convection in Porous Media," Springer-Verlag, New York.

[3] Dullien, F.A.L., 1992, "Porous Media: fluid Transport and Pore Structure," Academic Press.

[4] Tadrist, L., Miscevic, M., Rahli, O., and Topin, F., 2004, "About the Use of Fibrous Materials in Compact Heat Exchangers," Experimental Thermal and Fluid Science, Vol. **28**, pp. 193–199.

[5] Spielman, L. and Goren, S.L., 1968, "Model for Predicting Pressure Drop and Filtration Efficiency in Fibrous Media," Current Research, Vol. **2**, pp. 279-287.

[6] Choi, M.A., Lee, M.H., Chang, J., and Lee, S.J., 1999, " Permeability Modeling of Fibrous Media iIn Composite Processing," Journal of Non-Newtonian Fluid Mechanics, Vol. **79**, pp. 585-598.

[7] Mahjoob, S. and Vafai, K., 2008, "A Synthesis of Fluid and Thermal Transport Models for Metal Foam Heat Exchangers," International Journal of Heat and Mass Transfer, Vol. **51**, pp. 3701–3711.

[8] Gostick, J.T., Fowler, M.W., Pritzker, M.D., Ioannidis, M.A., and Behra, L.M., 2006, "In-plane and Through-Plane Gas Permeability of Carbon Fiber Electrode Backing Layers," Journal of Power Sources, Vol. **162**, pp. 228-238.

[9] Tomadakis, M.M. and Robertson, T., 2005, "Viscous Permeability of Random Fiber Structures: Comparison of Electrical and Diffusion Estimates with Experimental and Analytical Results," Journal of Composite Materials, Vol. **39**, pp. 163-188.

[10] Jackson, G.W. and James, D.F., 1986, "The Permeability of Fibrous Porous Media," Canadian Journal of Chemical Eng., Vol. **64**, pp. 364–374.

[11] Happel, J. and Brenner, H., 1973, "Low Reynolds Number Hydrodynamics," Noordhoff.

[12] Happel, J., 1959, "Viscous Flow Relative to Arrays of Cylinders," AICHE, Vol. **5**, pp. 174–177.

[13] Sparrow, E. M. and Loeffler, A. L., 1959, "Longitudinal Laminar Flow between Cylinders Arranged in Regular Array," AICHE, Vol. **5**, pp. 325-330.

[14] Drummond, J.E. and Tahir, M.I., 1984, "Laminar Viscous Flow through Regular Arrays of Parallel Solid Cylinders," International Journal of Multiphase Flow, Vol. **10**, pp. 515-540.

[15] Astrom, B.T., Pipes, R.B., and Advani, S.G., 1992, "On Flow through Aligned Fiber Beds and Its Application to Composite Processing," Journal of Composite Materials, Vol. **26** (9), pp. 1351-1373.

[16] Tamayol, A. and Bahrami, M., 2009, "Analytical Determination of Viscous Permeability Of Fibrous Porous Media," International Journal of Heat and Mass Transfer, Vol. **52**, pp. 3691-3701.

[17] Tamayol, A. and Bahrami, M., 2008, "Numerical Investigation of Flow in Fibrous Porous Media," ECI International Conference on Heat Transfer and Fluid Flow in Microscale, 21-26 September 2008, Whistler, Canada.

[18] Fluent 6.3 Users' Guide, 2007, Fluent Inc., Lebanon, USA.

[19] Bahrami, M., Yovanovich, M.M., and Culham, J.R., 2006, "Effective Thermal Conductivity of Rough Spherical Packed Beds," International Journal of Heat and Mass Transfer, Vol. **49**, pp. 3691-3701.

[20] Sadeghi, E., Bahrami, M., and Djilali, N., 2008, "Analytical Determination of Effective Thermal Conductivity of PEM Fuel Cell," Journal of Power Source, Vol. **179** (1), pp. 200-208.

[21] Clauge, D.S. and Philips, R.J., 1997, "A Numerical Calculation of the Hydraulic Permeability of Three-Dimensional Disordered Fibrous Media," Physics of Fluids, Vol. **9** (6), pp. 1562-1572.

[22] Kuwabara, S., 1959, "The Forces Experienced by Randomly Distributed Parallel Circular Cylinders or Spheres in a Viscous Flow at Small Reynolds Numbers" Journal of Physical Society of Japan, Vol. **14**, pp. 527-532.

[23] Hasimoto, H., 1959, "On the Periodic Fundamental Solutions of the Stokes Equations and Their Application to Viscous Flow Past a Cubic Array of Spheres," Journal of Fluid Mechanics, Vol. **5**, pp.317–328.

[24] Sangani, A.S. and Acrivos, A., 1982, “Slow Flow Past Periodic Arrays of Cylinders with Application to Heat Transfer,” International Journal of Multiphase Flow, Vol. **8**, pp.193–206.

[25] Sangani, A.S. and Yao, C., 1988, “Transport Processes in Random Arrays of Cylinders: II-Viscous Flow,” Physics of Fluids, Vol. **31** (9), pp. 2435-2444.

[26] Szaniawski, A., Lipnicki, Z., 2008, “Heat Transfer to Longitudinal Laminar Flow between Thin Cylinders,” International Journal of Heat Mass Transfer, Vol. **51**, pp. 3504–3513.

[27] Sobera, M.P. and Kleijn, C.R., 2006, “Hydraulic Permeability of Ordered and Disordered Single-Layer Arrays of Cylinders,” Physical Review E, Vol. **74**, pp. 036302-1-10.

[28] Farlow, S.J., 1993, “Partial Differential Equations for Scientists and Engineers,” Dover Publication INC., NY.

[29] Sullivan, R.R., 1942, “Specific Surface Measurements on Compact Bundles of Parallel Fibers,” Journal of Applied Physics, Vol. **13**, pp. 725-730.

[30] Skartsis, L., Khomami, B., and Kardos, J.L., 1992, “Resin Flow Through Fiber Beds During Composite Manufacturing Processes. Part II: Numerical and Experimental Studies of Newtonian Flow Through Ideal and Actual Fiber Beds,” Polymer Engineering and Sciences, Vol. **32**(4), pp. 231-239.